Unusual, high-temperature, iron-rich, mineral phases produced by natural burning of coal seams--Analytical data

J.R. Herring and P.J. Modreski

U.S. Geological Survey, Box 25046, MS 939, Denver, Colorado 80225

U.S. Geological Survey Open-File 87-22

ABSTRACT

During the Holocene, the natural combustion of coal seams in the western United States has produced large amounts of intensely altered sedimentary rock overlying the burning coal. This thermal alteration has heated the rocks to temperatures of 1300°C or higher, as inferred from the mineral assemblages. Such temperatures are achieved by no other common metamorphic process at atmospheric pressure. As a result the altered rocks contain unusual, high-temperature mineral phases. In cases of extreme high temperature, an iron-rich liquid slag forms, separates from the parent rock, and then accumulates by flowing into puddles. The slag specimens analyzed have an overall iron oxide content of 35-40 percent, with Fe^{+3} about ten times the abundance of Fe^{+2}. Chemically, the slag might be likened to an iron-rich basalt or andesite.

Conditions of intense heating coupled with rapid cooling are reflected in the mineralogy of the slag, with examples such as exsolution/oxidation lamellar intergrowths between hematite and magnetite, with Ti concentrated in the hematite, Mg in the magnetite, and both containing significant Al. At least four iron oxide phases can be identified in the slag. Flowing at slightly above its melting point, the slag forms drip-like structures where it flows into a cooler zone of the fire and quickly cools, preserving the shape of the drops. Fe-Mg oxide crystals located toward the outside of the slag droplets contain up to 15 weight percent ZnO. The likely source of the Zn is release from coal in or sediments adjacent to the burning seam; it is likely that other volatile trace metals from the coal may be incorporated into the slag as well.

The bulk iron content of the sedimentary rocks overlying the coal appears insufficient to produce the iron-rich slag; large quantities of these rocks with their relatively low and well-disseminated iron content would be needed. Instead, local enrichments of iron, such as in pyrite or iron-rich concretions in the rock overlying the coal, likely provided the iron to produce the slag.

INTRODUCTION

An unusual class of intensely altered rock is produced when ordinary sedimentary rock is thermally metamorphosed by the natural, in-situ combustion of underlying, thick coal seams. In the United States, this most commonly occurs in the low-rank coal basins of the Western States, described for example by Rogers (1918), but localities where this has occurred are known in other parts of the United States and at least 12 other countries as well (Bentor and others, 1981). The phenomenon also has been noted in association with the in-situ combustion of kerogen-rich (bituminous) shales described by Bentor and others (1981); but even so, these intensely altered rocks have received only cursory examination in the past. The combustion produces baked, brilliantly colored, erosion-resistant rock that commonly caps topographically high areas. The thermally altered rock commonly is called clinker, although it is also referred to as scoria, red dog, and slag. Previously, the term clinker has been defined specifically as material residual from coal combustion, but it is used here to refer to rocks overlying the burning coal that have been thermally altered in any way, including sintering or melting, as well as to material residual from the burning coal. Intensely heated rock can produce clinker that is sintered (Figure 1) or melted (Figure 2). For this latter material, various terms, such as paralava, appear in the literature for the fused, then cooled rock, but the preferred term in this study for the melted rock is slag, a term free of association with igneous rocks.

Rocks overlying the burning coal locally are heated intensely, some to temperatures well in excess of 1300°C, as inferred from the resulting mineral phase assemblages and field measurements. The atmosphere accompanying the heating ranges from oxidizing to mildly reducing, depending on residual oxygen and the amount of highly reducing combustion gases produced (Hooper, 1982). The mineral assemblage produced during the thermal metamorphism is determined by the initial composition of the sedimentary rock, combustion conditions including the highest temperature attained, and the cooling history. These rocks are of interest to petrologists, petrographers, and geochemists in that they represent examples of an extreme, heretofore little explored portion of the metamorphic P-T regime, wherein extremely high temperatures have been attained, but at or near atmospheric pressure. Other aspects of interest in these rocks involve their magnetic properties, which include extremely strong magnetic signatures, on the order of 5000 gammas. The rocks also are ideal for using fission track ages to measure rates of erosion and downcutting in landform development (Coates and Naeser, 1984); the ages are reset during the burning, which is contemporaneous with exposure.

In the Powder River Basin, Wyoming, the typical rock overlying coal seams is siltstone or silty shale, with sandstone less common. When baked by the heat of the burning coal, such rocks, now clinker, often remain in place, and retain evidence of their original sedimentary character and structure, although they become indurated and brick-like, with welded grains and conchoidal fracture when broken. Clinker commonly is highly fractured apparently as a result of heating. The clinker examined as a part of this study comes from the coal-producing sedimentary rocks of the Powder River Basin, notably the lowermost Wasatch and uppermost Fort Union Formations, of early Eocene and late Paleocene age, respectively. The clinker is most abundant towards the margins of the basin, where the coal seams tend to be shallow and, hence, have better access to air to support combustion than in

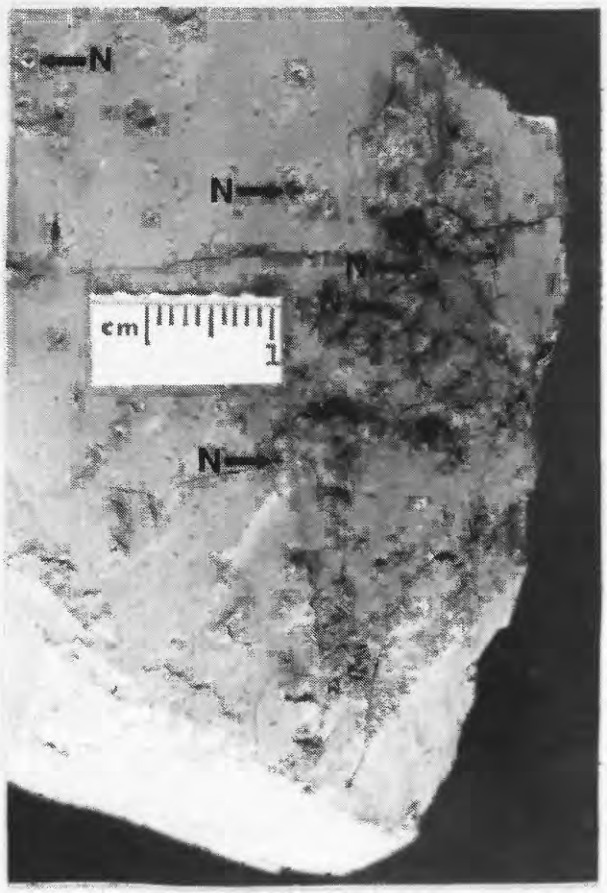

Figure 1. Photograph of baked, sintered shale (buchite), showing nodules of specular hematite (N in figure) presumably resulting from oxidative heating of small, framboidal pyrite nodules, 1-5 mm in size, in the original shale. Note the hollow centers typical of these nodules, resulting from the volume difference between pyrite and hematite for equal numbers of iron atoms.

a

b

Figure 2. Flow and drip structures of iron-rich slag produced by in situ heating of shale from combustion of underlying coal seams. In Figure 2b the tiny teardrops dripped onto a piece of baked shale in a cooler area where the droplets cooled and hardened. Specimen is correctly oriented as found, with up at top of photo. As the droplets cooled, tails of teardrops were still subject to heat, and being less rigid than the body, leaned over to produce the present shape.

the deeper coal seams. It is also at the margins of the basin where erosion and downcutting remain active and continue to expose near-surface coal seams facilitating combustion. In the areas of the basin margins where clinker is abundant, the resistant clinker beds are likely the controlling feature of landform evolution. The areal extent of clinker in the basin is estimated at between 10,000 and 20,000 km^2, with thickness ranging from a few to 100 m and averaging perhaps about 30 m. The average thickness of coal seam that has burned is estimated as 10 m, therefore approximately 10^{11} m^3, or about 200 billion tons, of coal has burned in the Powder River Basin.

Mineralogy of the thermally altered rock (clinker) indicates the extreme temperatures to which the rocks have been heated. In rocks heated to medium temperatures typical mineral assemblages include silica polymorphs (quartz, cristobalite, and tridymite), anorthite (An > 95%), iron-rich clinopyroxene (Cosca and others, 1985), and oxides of iron. Extreme temperatures produce highly altered rocks that contain high-temperature minerals such as hercynite and indialite, a high-temperature dimorph of cordierite. In the most extreme cases of heating, mullite has been formed by a process wherein the common rock-forming cations have been volatilized, leaving behind a crystalline residue of silicon-aluminum oxide. In addition, extremely high temperatures have produced interesting textural features, such as exsolution lamellae of unusual composition in the iron oxides.

Rocks subjected to the highest temperatures produce an iron-rich melt as a slag that segregates from the host rock. The material appears to have had low viscosity compared to most lavas, and it flows readily under gravitational influence. Where sufficient slag occurs, the material runs together in rivulets, which combine and form drip or flow structures (Figure 2) in the cracks and cavities produced by shrinkage of the host rock upon heating. The slag is dark, usually vesicular, and resembles a basalt in appearance and composition. However, a principal difference from ordinary basalt is that the slag has been heated to temperatures at least 100°C higher than normal temperatures of lava extrusion, which seldom exceeds 1200°C (Carmichael and others, 1974). In some cases the temperature may have been considerably higher. It is these high-temperature, iron-rich slags that are the focus of interest in this paper.

COMBUSTION CONDITIONS AND ENVIRONMENT

Coal ignition can occur from a variety of causes. The clinker used in this study was collected from the Powder River Basin, Wyoming, a region containing coal known for its tendency to spontaneously ignite (Herring and Rich, 1983). Direct ignition of the coal by lightning is probably rare; more likely is the symbiotic relationship between lightning-ignited, grass or brush fires, which ignite coal seams at the outcrop. The coal seam fires can burn or smolder for years and then become an ignition source for subsequent grass fires, which further can ignite additional coal seam fires.

The temperatures attained in natural combustion of coal, while high for surface geologic processes, are not particularly high compared to those in industrial combustion of coal. A typical combustion temperature in pulverized coal electrical power plants is around 1600°C, but this is attained using finely pulverized coal injected into the burner with an optimum, stoichiometric amount of oxygen in order to sustain and produce total combustion (Ceely and Daman, 1981). In natural, in-situ coal combustion the burning conditions are far less ideal and the temperatures perhaps lower; nevertheless, temperatures of natural coal burns are still remarkably high compared to common geologic processes at the Earth's surface.

Thick coal seams (as thick as 70 m in parts of the Powder River Basin prior to burning) leave structures in the altered rock after burning that provide some idea of combustion conditions. The intensity of heating is indicated by the formation of slag with associated flow structures, while slickensides and chaotic orientation of blocks of shale heated to form buchite reveal the collapse of the rocks into rubble-filled voids left behind by the burning of the underlying coal. Chimneys in the clinker show that the hottest exhaust gases were confined to localized areas.

Fire can consume the entire thickness of the coal seam or only part of the seam, usually the top, leaving behind unburned coal. A single locality may show that coal has burned over an areal extent hundreds of square kilometers, but it is unlikely that the entire area was on fire at one time. The burn more likely occurred as several local, perhaps unconnected, fires that moved on the order of a few meters per year. Fires might extinguish only to rekindle later when proper conditions again exist for ignition.

As the coal burns, it reduces in size to an ash of approximately one-tenth of the original volume of the coal. The ash comprises mostly the inert mineral matter originally in the coal. This volume reduction over the thickness of the coal seam removes the support of rocks overlying the seam and allows them to subside. Cavities left from the coal combustion fill with fragments of the collapsed, overlying rocks.

During the most intense combustion, cavities in the burn reach temperatures exceeding 1300°C as indicated by the altered minerals (discussed later), and by our heating experiments on naturally produced slag, indicating temperatures of 1267°C+. Field measurements confirm these hot temperatures. We measured a combusting coal seam at an abandoned, underground coal mine at 1140°C, using optical pyrometery. This temperature was measured in a subsidence cavity only 2 m below the ground surface; in the actual coal seam, approximately 20 m underground, temperatures undoubtedly were much higher. Burning coal seams are stoked by drafts of air rushing into the combustion cavity to replace air that is combusted or removed upward by convecting gases and heat from the burn. Cracks in the rocks above the burn, produced by failure and subsidence of overlying rock into the void left by the burning

coal, become the exhaust vent (chimney) for heat and combustion gases. After passage of the burn front, these subsidence cracks in the now cooled, highly fractured rock serve as an excellent intake manifold, which the air can enter to support further combustion. Jet-like convection cells are established, with intense velocities in the combustion-supporting air and the upward-convecting exhaust gases. In analogy to bellows used on a fire, the rapid convection furnishes abundant air to the burning coal and produces extremely hot temperatures. It is in the chimneys of the clinker where the greatest heat and consequent greatest thermal alteration of rock occur. When air supply is limited, combustion temperatures are kept much cooler and produce less thermal alteration of the overlying rock.

Gases emitted during burning reflect the combustion conditions. Abundant air supply produces very hot burning, which usually leads to complete combustion of the coal. The combustion product gases in this case would be carbon dioxide along with any unused, residual oxygen from the air, as well as the inert atmospheric gases. Limited air supply produces lower temperatures with possible incomplete combustion of the coal and the product gases are mixtures of carbon monoxide and dioxide (Herring, 1986). If large partial pressures of carbon monoxide exist, the combustion environment will be highly reducing and will greatly affect iron valence and mineralogy in the slag.

Rocks cool once the burn terminates. The burn can extinguish from passage of the fire front, exhaustion of the fuel, inadequate air supply, or suffocation resulting from collapse of overlying rock. Cooling in the case of rocks heated from natural coal fires occurs much more quickly than in the usual conduction-limited case for cooling of surficial igneous rock. In the case of natural coal burns, the heat is quickly lost by advection through the subsidence cracks that were created during burning. Rapid cooling results in the coexistence of metastable mineral assemblages that otherwise would not occur. An example of this is the relatively common co-occurrence in the slag and associated rocks of the silica polymorphs: quartz, cristobalite, and tridymite. Also, little glass occurs in these rocks. Hence, the cooling was sufficiently rapid that an equilibrium mineral assemblage was not produced, but not so rapid to quench the bulk of the slag to glass.

The age of combustion in Western United States coal seam fires is geologically very young. Fission track dating of reset zircons in baked sandstones commonly indicates burning ages of 1 to 2 million years or less for localities in the Powder River Basin (Coates and Naeser, 1984). In the slag from the Jacobs Ranch Coal Mine analyzed as a part of this study, there were no fission tracks in zircons in overlying, baked sandstone, indicating a combustion age of younger than 80,000 years. In many cases, the fires have been active during the past 2 centuries: historical documents from settlers mention the burns. Thus, the baked rocks discussed in this study can be considered as extremely recent; resultant mineral assemblages produced from the thermal alteration also can be considered to be fresh, with little or no opportunity for subsequent alteration during weathering.

ANALYSIS OF THE IRON-RICH SLAG

Most of the analyses of slags in this report are based on rocks collected from the strip mine pit of the Jacobs Ranch Coal Mine, south of Gillette, Wyoming. Extremely fresh exposure and accessible sections through the clinker, as much as to 40 m thick, occur at this locality. Much of the chemical and mineralogical analysis for this work has been done on slag occurring as a single cluster of teardrop shapes (Figure 2), each droplet about 1-cm diameter, taken from a chimney at this locality. In order to provide a homogeneous sample of what otherwise could be an extremely heterogeneous rock, the droplets were scraped free of any surface oxidation and ground-water deposits, then ground to less than 80 mesh and well mixed. This allowed similar, uniform composition samples to be analyzed and then compared using X-ray diffraction, Mossbauer spectrometery, and determinations of bulk chemistry. In addition, whole droplets from the cluster were sectioned and examined using electron microprobe analysis along with scanning electron and optical microscopy. Analysis of the sectioned droplets permitted observation of textural features and internal zoning. The teardrops vary in porosity from 20 to 40 percent, visual estimate, due to numerous spherical vesicles probably originating from gas bubbles when the drops were molten. These small cavities of approximately 0.1 to 1 mm diameter occur throughout the teardrops. In most droplets the vesicles are smaller and less abundant in the interior, compared to the outer few millimeters, though some contain a concentration of large vesicles near the center. Towards the exterior of the droplet commonly there is a concentration of the largest vesicles, which sometimes have coalesced to form hollow zones 2 to 10 mm long and about 1 mm deep.

The mineralogy of the vesicular droplets comprises iron oxides, laths of anorthite, about 50-100 μm in length, and a fine-grained groundmass of intergrown quartz and other silica polymorphs plus glass and possibly some potassium feldspar. Some patches in the groundmass are composed of brownish, partly devitrified or undevitrified glass. The iron oxides are dominantly magnetite and hematite, in subhedral to euhedral crystals about 5 to 100 μm in size, with the two minerals commonly being intergrown. Magnetite is more abundant in the interior of the droplets and hematite is the dominant iron oxide toward the outside. The magnetite contains a notable amount of Al and Mg, and commonly contains oriented exsolution lamellae of hercynite spinel, $(Fe,Mg)Al_2O_4$. The hematite is titaniferous (0-8 weight percent TiO_2) and also contains up to 7 weight percent Al_2O_3. The droplets have an iron oxide rim about 20 to 100 μm thick composed mainly of hematite plus a subordinate amount of magnesioferrite spinel that contains 1 to 15 weight percent ZnO.

The bulk mineralogy of the teardrops, determined by X-ray diffraction, comprises quartz, cristobalite, tridymite, nearly pure anorthite (An > 95%), hematite, and magnetite as major components (Figure 3). In the vugs of the teardrops, these same minerals occur along with minor amounts of calcium phosphate (apatite?) and clinopyroxene. The acicular crystals of clinopyroxene occurring in the vugs would be inferred to have an atomic composition of $Fe_{55}Mg_{15}Ca_{30}$, based on their optic angle of 49° using standard determinative curves. This clinopyroxene normally would be classified as ferroaugite; however, Cosca and others (1985) have shown that the pyroxenes in similar slags may range in composition from $CaMgSi_2O_6$ to near end member $CaFe^{+3}AlSiO_6$ and, because of this range, the standard determinative curves may not apply. Crystals in the matrix of the teardrop range in length from 5 to

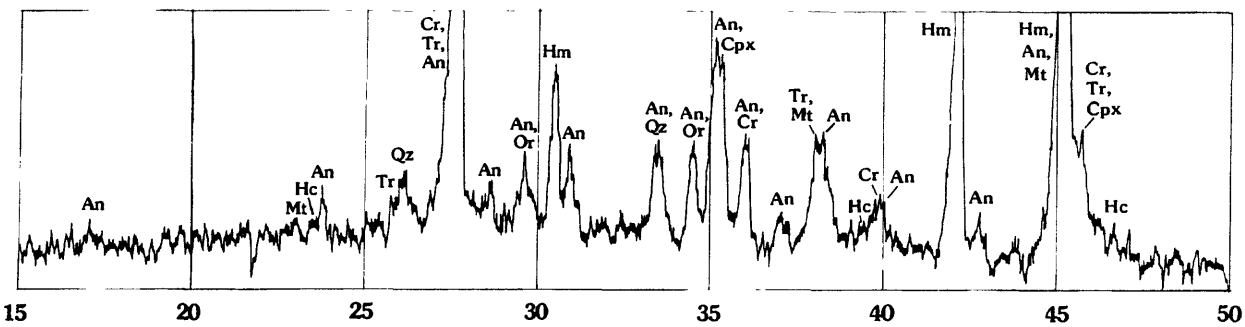

FIG. 3 DEGREES 2-THETA Fe K-ALPHA

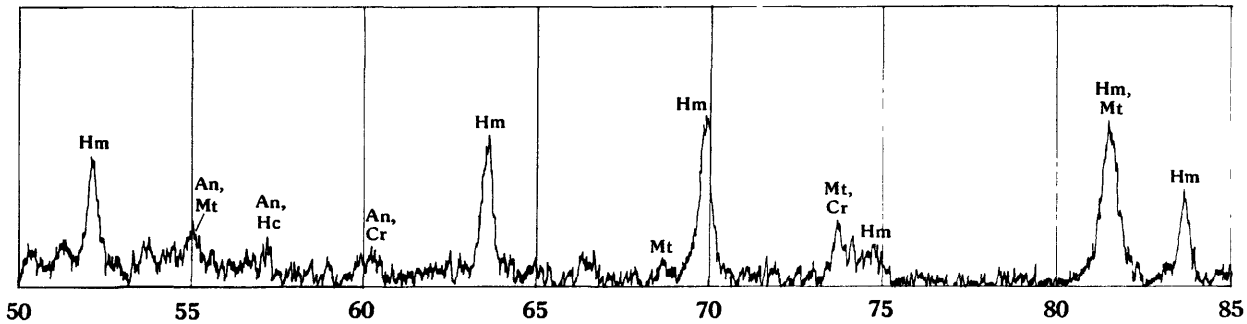

Figure 3. X-ray diffraction pattern of bulk mineralogy of crushed and ground teardrops. Scan was run using nickel-filtered, iron Kα radiation to minimize fluorescence of iron in the sample. The scan was run at $2^{o}2\Theta$ per minute. Minerals identified are: Qz-quartz, Hm-hematite, Mt-magnetite and/or magnesioferrite, Hc-hercynite, An-anorthite, Cpx-clinopyroxene, Or-orthoclase, Cr-cristobalite, and Tr-tridymite. An X-ray scan of the highly baked shale showed most of these same minerals along with readily identifiable cordierite and mullite.

100 μm, while the smaller crystals in the vugs usually are less than 1 mm.

Bulk chemical composition of the teardrops is shown in Table 1 and compared with a representative basalt for which trace element data are available. The CIPW normative compositions based on the bulk chemistry of the slag and a representative basalt are given in Table 2. Preliminary analysis of the iron valances in the ground teardrop composite using Mossbauer spectroscopy showed apparently equal proportions of +2 and +3 states; however, subsequent analysis using X-ray fluorescence and wet chemistry showed that the actual ferric/ferrous ratio was closer to 10. Elemental iron was not detected in this material, although it has been reported in rocks overlying artificial, in-situ-gasification coal burns where the pO_2 was kept low in order to ensure production of a burnable product gas (L. Burns, oral commun., 1986; and Craig and others, 1982). The composition of the bulk teardroplets is quartz- and corundum-normative. Much of the Al_2O_3 and MgO, appearing in the normative composition as corundum and hypersthene, are in the actual droplet contained in solid solution in the magnetite and hematite. In its composition of major elements, the slag is richer in iron and poorer in Si, Mg, Ca, and Na relative to average basalt. The normative composition of the slag reflects its enrichment in Fe_2O_3 relative to the basalt. The corundum-normative component of the slag results from the low CaO content and reflects the origin of the slag from aluminum-rich shale. The large amount of normative quartz in the slag results from the relative paucity of MgO, CaO, and FeO. Higher concentrations of these three oxides in the slag would otherwise be expressed as pyroxenes, both in the actual mineralogy and the normative composition.

Table 3 lists the trace element composition of the slag along with a representative basalt. Comparative trace element enrichment in the slag, again relative to the basalt, exists for Pb, Y, P, and Zn; the slag is somewhat depleted in Ni. Based on the abundance of La and Ce, there is some suggestion that the lanthanide rare earth elements may be enriched in the slag.

Representative microprobe analysis of major element composition of the various iron oxide phases is given in Tables 4 to 9. The microprobe conditions for the analyses are given in the Appendix to this report, along with identification of the various point analyses and droplet identification. Tables 4 and 5 list individual hematite analyses, as well as averages representative of the different compositions of hematite present in the droplets. The TiO_2 content of the hematite ranges from near 0 to 7.5 weight percent and Al_2O_3 in the same minerals ranges from about 0.5 to 6.5 weight percent. The hematite phases apparently are zoned within the droplet--the hematite that is low in Ti and Al occurs towards the droplet rim (Figure 4).

Representative analyses of the magnetite are given in Tables 6 and 7. Magnetite in the outer part of a droplet is a homogeneous, single-phase mineral, but towards the droplet center it contains an increasing abundance of exsolution lamellae of hercynite-rich spinel. A typical structural formula, based on a total of three cations per formula unit and calculating Fe^{+3}/Fe^{+2} to give four total oxygen atoms, for the homogeneous magnetite in the outer part of the sample is (analysis MtX4H):

$$(Mg_{0.15}Mn_{0.01}Fe^{+2}_{0.84})_{\Sigma 1.00}\ (Fe^{+3}_{1.63}Al_{0.35})_{\Sigma 1.98}\ O_{4.00}$$

Analysis of the hercynite lamellae was difficult because of the narrowness, about 1 μm maximum, of the lamellae; most of the analyses (given in Table 8) probably include some overlap with the host magnetite. The structural formula

Table 1.--Percent oxide analysis of major and minor elements in ground, homogenized teardrops compared with a representative basalt

[Analytical techniques are X-ray Fluorescence (XRF) and Inductively Coupled Plasma spectrometry (ICP). Note: The FeO analysis listed in the XRF analysis was performed by wet chemistry. Total Fe was determined using XRF, and Fe_2O_3 was calculated by difference. Oxide values from the ICP analyses, expressed in weight percent are included for comparison with the X-ray fluorescence analysis. The relatively low total iron value measured by ICP, compared to that measured by XRF, is an artifact of the semiquantitative nature of the ICP technique. The XRF analysis should be accepted as accurate for total iron as well as the other major and minor elements. Total for the ICP technique is not included because in the technique Si is not determined (n.d.). Analysis of a basalt from the Talasea volcanic field, New Britain (Lowder and Carmichael, 1970), for which trace element data also are available (see Table 3), is included for comparison]

	XRF	ICP	Basalt
SiO_2	40.3	n.d.	51.57
Al_2O_3	13.5	11.7	15.91
Fe_2O_3	32.9	--	2.74
FeO	2.37	--	7.04
Total Fe [as Fe_2O_3]	[35.5]	16.7	[10.48]
MgO	2.2	1.8	6.73
CaO	5.0	4.2	11.74
K_2O	1.0	0.8	0.44
TiO_2	0.5	0.2	0.80
P_2O_5	1.3	1.0	0.11
MnO	0.3	0.3	0.17
Na_2O	<0.2	0.2	2.41
Loss on ignition	0.55	--	0.45
Total	99.9	--	100.11

Table 2.--CIPW normative composition of the iron-rich teardrop based on the chemical analysis determined by XRF and wet chemistry (Table 1)

[The basalt, whose bulk composition is given in Table 1, is included for comparison]

	Slag	Basalt
Q	26.17	2.24
Or	5.90	2.62
Ab	--	20.40
An	16.27	31.27
Hy	5.48	16.06
Di	--	21.30
Mt	7.15	3.98
Hm	27.93	--
Il	0.96	1.52
Ap	3.09	0.27
C	6.45	--
Total	99.40	99.66

Table 3.--Semiquantitative analysis of trace elements in parts per million of the crushed teardrops using inductively coupled plasma (ICP) emission spectroscopy

[Element concentrations shown as less than, <, are present but below the detection limit of the analytical technique, which appears following the < symbol. The representative basalt is described in Table 1. Nb in the basalt was looked for but not detected]

Element	Iron-rich slag	Basalt
Ba	510	150
Be	3	
Cd	10	
Ce	64	35
Co	3	
Cr	27	125
Cu	27	175
Ga	<20	15
La	35	15
Li	15	
Mo	5	
Nb		<20
Ni	15	100
Pb	45	1
Sc	8	
Sn	<20	
Sr	150	355
Ta	<50	
Th	<10	15
U	<200	
V	74	275
W	<10	
Y	52	
Zn	490	80

Table 4. Microprobe analyses of hematite associated with magnesioferrite near rim of teardrop

[Numbers in parentheses under the column headings are the number of points combined to produce the averages in the table. Zeros in square brackets are analyses statistically insignificant from 0. The microprobe analysis measured total iron; FeO and Fe_2O_3 values are those calculated to give a stoichiometric formula with 4 oxygen atoms and a total of 3 cations]

	HmF2 (2)	HmX1 (3)	HmE1 (2)	HmF1 (2)	HmY2 (3)	HmC1 (2)	HmY3 (1)	HmX2 (2)	HmY1 (2)
ZnO.....	[0]	[0]	[0]	[0]	[0]	[0]	[0]	[0]	[0]
MgO.....	0.16	0.16	[0]	0.10	[0]	0.16	0.11	0.06	0.07
CaO.....	0.08	0.04	0.14	0.12	[0]	0.04	0.21	0.04	0.04
MnO.....	0.26	0.42	0.04	0.24	0.23	0.26	0.03	0.04	0.18
Al_2O_3.....	0.42	0.49	2.53	0.81	0.68	0.69	2.54	3.30	0.87
TiO_2.....	0.04	0.04	0.04	0.05	0.05	0.10	0.13	0.18	0.28
SiO_2.....	[0]	[0]	[0]	[0]	[0]	[0]	0.11	0.12	[0]
Fe_2O_3.....	97.86	98.73	96.71	98.78	97.88	98.93	93.44	96.23	98.35
Total.....	98.88	99.97	99.56	100.16	99.08	100.18	96.57	100.03	99.79

Table 5. Microprobe analyses of hematite associated with magnetite in the interior of the teardrop

[Numbers in parentheses under the column headings are the number of points combined to produce the averages in the table. Zeros in square brackets are analyses statistically insignificant from 0. The microprobe analysis measured total iron; FeO and Fe_2O_3 values are those calculated to give a stoichiometric formula with 4 oxygen atoms and a total of 3 cations]

	HmH1 (3)	HmX3 (4)	HmD2 (2)	HmY4 (2)	HmG1 (2)	HmD3 (2)	HmJ1 (2)	HmD1 (2)	HmG2 (2)	HmX6 (2)	HmI1 (2)	HmX4 (4)	HmK1 (2)	HmA2 (2)	HmA1 (3)	HmX5 (3)
ZnO....	[0]	[0]	[0]	[0]	[0]	[0]	[0]	[0]	[0]	[0]	[0]	[0]	[0]	[0]	[0]	[0]
MgO.....	0.23	0.25	0.28	0.29	0.54	0.53	0.58	0.48	0.60	0.44	0.56	0.40	0.38	0.50	0.62	0.49
CaO.....	0.15	0.08	0.14	0.07	0.10	0.12	0.14	0.12	0.13	0.10	[0]	0.05	[0]	[0]	[0]	0.03
MnO.....	0.09	0.05	0.04	0.06	0.07	0.03	0.04	0.05	0.08	0.04	0.04	0.05	0.06	0.04	0.06	0.05
Al_2O_3...	3.88	5.31	5.06	4.54	4.53	5.20	4.22	5.04	6.59	4.94	4.07	4.22	3.94	3.93	4.18	3.89
TiO_2....	0.55	1.62	2.82	3.08	3.70	4.17	4.51	4.62	4.83	5.41	5.50	5.56	6.06	6.44	7.47	7.56
SiO_2....	0.13	0.30	0.08	0.14	0.08	[0]	0.11	0.09	0.13	0.16	[0]	0.14	[0]	[0]	0.17	0.09
Fe_2O_3..	94.85	91.10	90.44	88.96	91.01	90.21	90.05	89.11	87.76	89.53	90.31	90.40	88.73	88.15	87.06	87.91
Total..	99.88	98.76	99.07	97.04	100.03	100.46	99.72	99.56	100.12	100.66	100.51	100.88	99.40	99.10	99.57	100.02

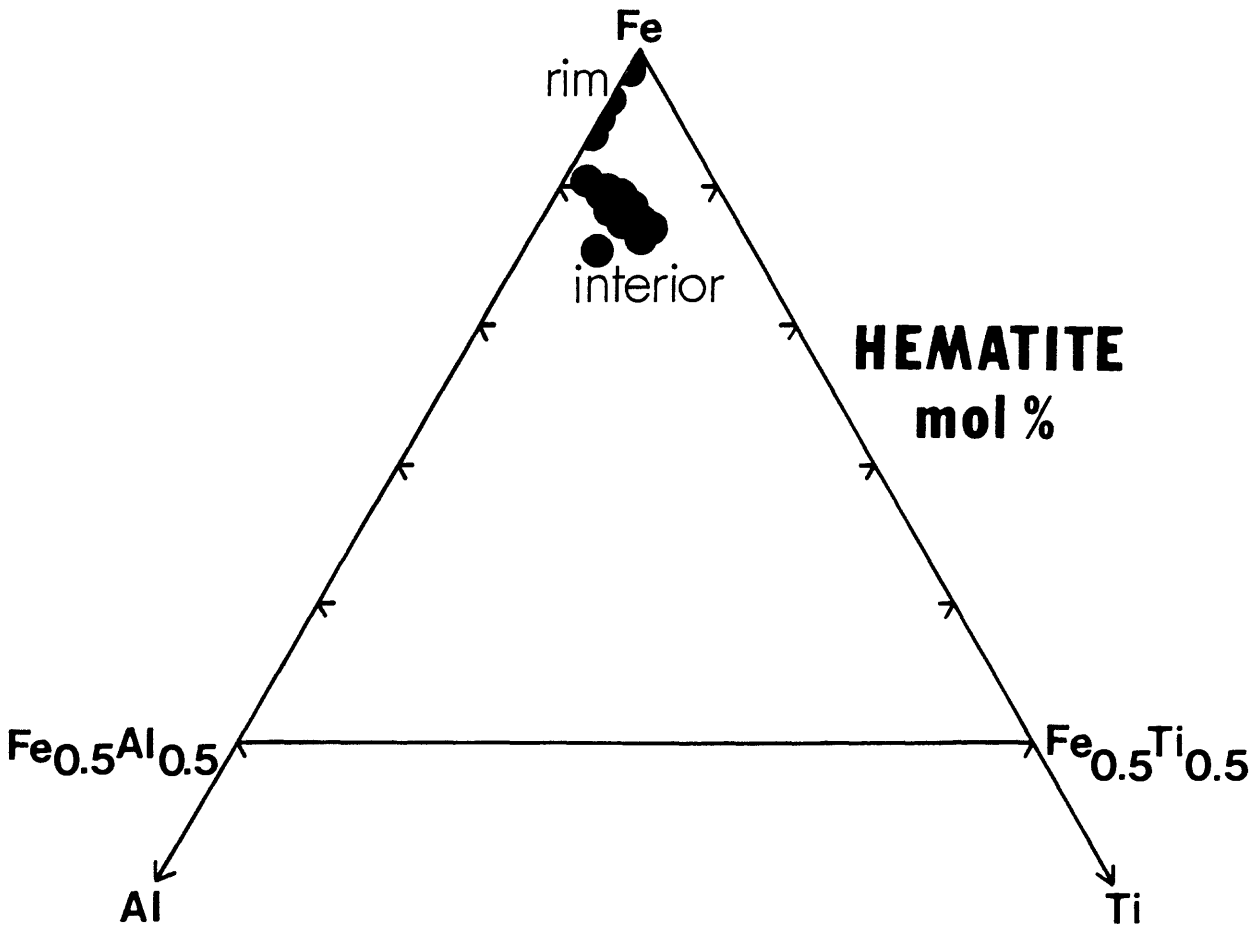

Figure 4. Triangular Fe-Al-Ti plot, in mole fraction, of hematite compositions, computed from microprobe analyses. Only the Fe-rich half of the Fe-Al-Ti ternary diagram is shown. Points nearest the Fe vertex (rim) are compositions of hematite associated with magnesioferrite and zincian magnesioferrite near outer rim of teardrop. Points with about 85 to 90 mole percent Fe (interior) are hematite associated with magnetite in interior of the teardrop.

Table 6. Microprobe analyses of magnetite phases

[The analyses are of lamellae-free host magnetite within the host plus spinel intergrowths, except for sample MtX5, which is an exsolution-free, single-phase magnetite. Numbers in parentheses under the column headings are the number of points combined to produce the averages in the table. Zeros in square brackets are analyses statistically insignificant from 0. The microprobe analysis measured total iron; FeO and Fe_2O_3 values are those calculated to give a stoichiometric formula with 4 oxygen atoms and a total of 3 cations]

	MtK82 (1)	MtX4H (2)	MtK73 (1)	MtX3H (1)	MtL84 (1)	MtX5 (3)
ZnO	0.37	0.13	[0]	0.32	0.46	0.14
MgO	1.06	2.84	2.71	3.45	2.87	2.70
CaO	0.07	0.04	0.08	0.07	0.16	[0]
MnO	0.40	0.48	0.39	0.50	0.62	0.46
Al_2O_3	4.64	8.43	9.81	11.19	12.60	10.77
TiO_2	0.23	0.17	0.18	0.06	0.08	0.18
SiO_2	[0]	0.10	[0]	0.11	[0]	[0]
FeO	30.32	28.03	28.69	28.08	28.67	28.78
Fe_2O_3	65.24	60.59	59.52	59.69	57.81	58.38
Total	102.33	100.81	101.38	103.47	103.27	101.41

Table 7. Microprobe analyses of combined magnetite host plus spinel exsolution lamellae, averaged by using broad electron beam.

[Numbers in parentheses under the column headings are the number of points combined to produce the averages in the table. Zeros in square brackets are analyses statistically insignificant from 0. The microprobe analysis measured total iron; FeO and Fe_2O_3 values are those calculated to give a stoichiometric formula with 4 oxygen atoms and a total of 3 cations]

	MtX4 (4)	MtD2 (3)	MtB1 (3)	MtX3 (6)	MtA1 (3)	MtD1 (2)	MtI1 (3)	MtD3 (3)	MtG1 (4)	MtK1 (3)	MtJ1 (2)	MtY4 (1)	MtH1 (5)
ZnO.....	0.19	[0]	0.22	0.26	0.33	[0]	[0]	0.23	0.34	[0]	0.31	0.40	0.75
MgO.....	3.50	4.92	4.75	4.15	4.43	5.72	6.00	7.36	6.48	4.80	6.23	6.15	16.73
CaO.....	0.04	0.07	[0]	0.07	[0]	0.16	0.05	0.11	0.08	[0]	0.06	[0]	0.11
MnO.....	0.50	0.66	0.44	0.56	0.47	0.61	0.55	0.64	0.68	0.42	0.52	1.04	2.35
Al_2O_3.....	11.67	12.41	13.92	14.73	14.78	15.03	16.72	16.90	16.97	17.29	17.65	20.71	21.72
TiO_2.....	0.21	[0]	0.17	0.07	0.21	[0]	0.06	[0]	[0]	0.34	0.12	0.08	[0]
SiO_2.....	0.09	[0]	0.08	0.08	[0]	0.11	0.16	0.18	0.10	0.10	[0]	[0]	0.15
FeO.....	27.62	25.44	26.48	27.30	26.97	25.00	25.28	22.80	23.37	26.94	25.02	23.67	6.00
Fe_2O_3.....	57.28	58.30	56.20	55.32	55.22	55.94	54.07	54.61	52.94	50.87	54.12	46.34	51.88
Total.....	101.10	101.80	102.26	102.54	102.41	102.57	102.89	102.83	100.96	100.76	104.03	99.39	99.69

Table 8. Analyses of predominantly spinel exsolution lamellae, principally hercynite, plus a variable amount of overlap by host magnetite

[Numbers in parentheses under the column headings are the number of points combined to produce the averages in the table. Zeros in square brackets are analyses statistically insignificant from 0. The microprobe analysis measured total iron; FeO and Fe_2O_3 values are those calculated to give a stoichiometric formula with 4 oxygen atoms and a total of 3 cations]

	HcK83 (1)	HcK80 (1)	HcK79 (1)	HcL1 (1)	HcX1 (1)
ZnO	[0]	0.48	0.34	0.98	0.70
MgO	2.41	1.61	8.65	5.72	11.56
CaO	0.06	[0]	[0]	0.21	0.04
MnO	0.53	0.47	0.55	0.26	0.54
Al_2O_3	23.12	29.71	38.19	48.53	48.61
TiO_2	0.24	0.35	0.21	0.25	0.06
SiO_2	0.13	[0]	[0]	0.25	0.21
FeO	33.31	36.11	23.80	31.72	22.00
Fe_2O_3	47.09	40.70	28.42	17.94	19.92
Total	106.89	109.43	100.16	105.86	103.64

for the analysis of a hercynite spinel lamella showing the least Fe and highest Mg and Al is (analysis HcX1):

$$(Mg_{0.47}Zn_{0.01}Mn_{0.01}Fe^{+2}_{0.51})_{\Sigma 1.00}\ (Fe^{+3}_{0.41}Al_{1.57}Si_{0.01})_{\Sigma 1.99}\ O_{4.00}$$

A typical formula for the averaged composition of host magnetite plus lamellae, obtained by broadening the microprobe beam to about 20 µm diameter, for the grains in the interior is (analysis MtG1):

$$(Fe^{+2}_{0.65}Mg_{0.32}Mn_{0.02}Zn_{0.01})_{\Sigma 1.00}\ (Fe^{+3}_{1.33}Al_{0.67})_{\Sigma 2.00}\ O_{4.00}$$

Spinel near the rim of the teardrops shows an unusual enrichment in zinc. The oxide phase occurring in the outer 100 µm of the droplet is a magnesioferrite spinel, ideally $MgFe_2O_4$, which contains up to 15 weight percent ZnO (Table 9). The Zn content of this spinel increases outward, from about 0.5 weight percent ZnO at the inner portion of the rim to its maximum value at the rim surface. This zinc-bearing spinel is intergrown with hematite that is nearly pure Fe_2O_3 (Table 4). The Zn is present throughout the entire magnesioferrite grain and, hence, must be incorporated in the lattice rather than simply adsorbed on the surface. The source of the Zn is no doubt volatilization and removal from the coal and/or coal-associated sediments, which have typical Zn concentrations of 30 and 100 ppm, respectively. The Zn was transported in the combustion gases and incorporated into the teardrops probably as temperature began decreasing.

A calculated stoichiometric formula of the low-zinc magnesioferrite (analysis MfC2) is:

$$(Mg_{1.05}Mn_{0.06}Zn_{0.01})_{\Sigma 1.12}\ (Fe^{+3}_{1.76}Al_{0.11})_{\Sigma 1.87}\ O_{3.94}$$

The formula can be improved by expressing part of the Mn as +3 to account for the small deficiency in oxygen; this gives the formula

$$(Mg_{1.05}Zn_{0.01})_{\Sigma 1.06}\ (Fe^{+3}_{1.76}Al_{0.11}Mn^{+3}_{0.06})_{\Sigma 1.93}\ O_{3.97}$$

An average formula for the high-zinc magnesioferrite (analysis MfF1) is:

$$(Mg_{0.62}Ca_{0.01}Zn_{0.40})_{\Sigma 1.03}\ (Fe^{+3}_{1.78}Al_{0.12}Mn^{+3}_{0.07})_{\Sigma 1.97}\ O_{3.99}$$

Magnesioferrite spinel containing these large amounts of Zn is an unusual composition and, to our knowledge, has not been observed in any other natural rocks.

Compositions of spinel phases, in mole percent, are plotted in the spinel quadrilateral $MgAl_2O_4$-$FeAl_2O_4$-$FeFe_2O_4$-$MgFe_2O_4$ in Figure 5 for rim (magnesioferrite), host (magnetite free of lamellae), exsolution lamellae, and averaged magnetite plus lamellae analyses. Figure 6 is a plot of the divalent cation content of the spinels, plotted in the system MgO-FeO-ZnO for rim (magnesioferrite) and interior (both homogeneous magnetite and magnetite plus hercynite lamellae) compositions.

Other volatile metals present in the Powder River Basin's coal, with concentrations in ppm given for the whole coal (Hobbs, 1980), include As (5), Hg (0.1), Sb (0.5), Se (1), Cd (0.1), F (70), and Pb (4). These and other volatile metals, such as Sn, are known to occur in condensate minerals associated with coal mine fires in the Eastern (Lapham and others, 1980) and Western (Herring, 1986) United States. It is likely that, upon further

Table 9. Magnesioferrite averages

[Numbers in parentheses under the column headings are the number of points combined to produce the averages in the table. Zeros in square brackets are analyses statistically insignificant from 0. The microprobe analysis measured total iron; FeO and Fe_2O_3 values are those calculated to give a stoichiometric formula with 4 oxygen atoms and a total of 3 cations]

	MfC2 (2)	MfC1 (2)	MfY5 (2)	MfE1 (3)	MfX1 (4)	MfY4 (2)	MfY3 ((3)	MfY2 (2)	MfY1 (3)	MfF2 (2)	MfF1 (2)
ZnO	0.58	0.82	1.16	1.25	2.09	6.64	9.45	10.32	13.56	15.18	15.50
MgO	21.72	21.72	19.26	21.49	17.75	15.67	14.83	14.30	12.52	12.62	11.94
CaO	[0]	[0]	0.08	0.07	0.03	0.07	[0]	[0]	[0]	0.09	0.26
MnO	2.30	2.32	1.91	1.79	2.52	2.65	2.62	2.46	2.26	2.35	2.44
Al_2O_3	2.90	2.40	10.34	12.19	2.03	2.80	2.62	2.02	2.04	2.70	2.96
TiO_2	[0]	[0]	[0]	[0]	[0]	[0]	0.06	[0]	[0]	[0]	[0]
SiO_2	[0]	0.08	[0]	0.14	[0]	[0]	[0]	[0]	[0]	[0]	[0]
FeO	0.00	0.00	0.00	0.00	0.00	0.00	0.00	0.00	0.00	0.00	0.00
Fe_2O_3	72.33	72.61	65.74	63.08	74.06	64.28	62.67	69.85	68.70	67.55	68.39
Total	99.83	99.95	98.59	100.01	98.51	99.27	99.23	99.07	99.08	100.49	101.49

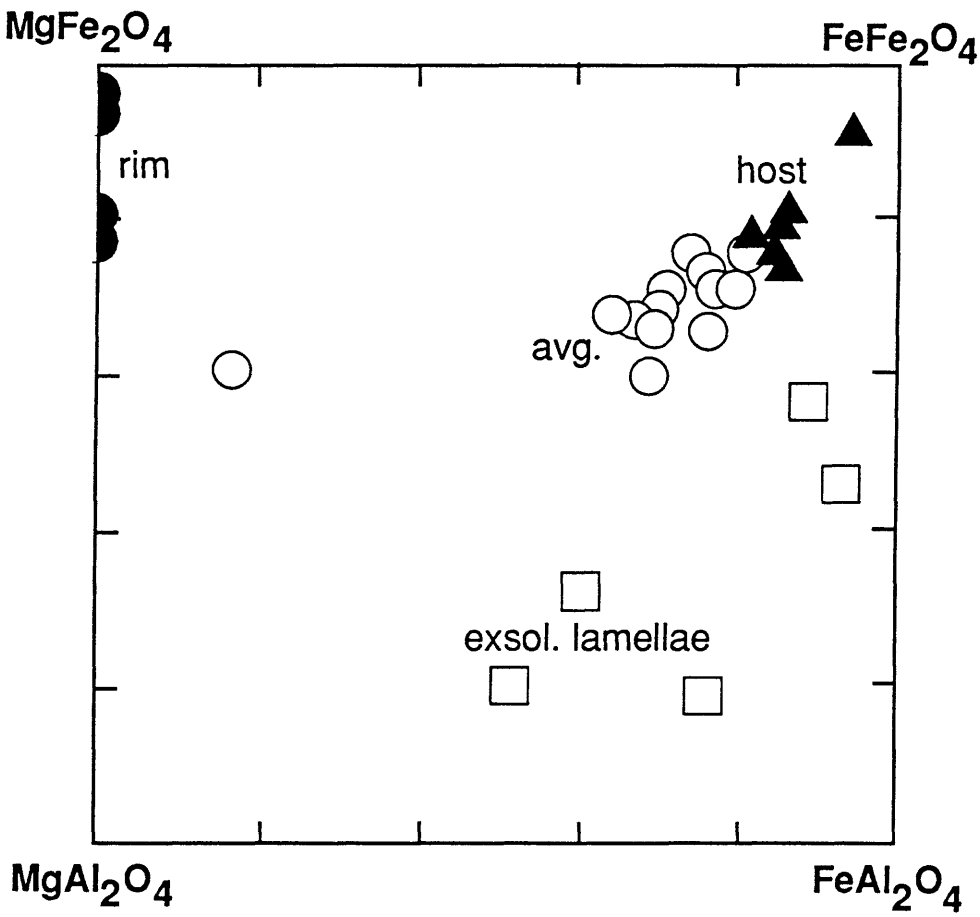

Figure 5. Plot of compositions, in mole fractions, of spinels, from structural formulae computed from microprobe analyses, within the spinel quadrilateral $MgAl_2O_4$-$FeAl_2O_4$-Fe_3O_4-$MgFe_2O_4$. Solid circles near $MgFe_2O_4$ vertex (rim) are magnesioferrite spinels from rim of teardrop. Squares in lower part of diagram (exsolution lamellae) are analyses of hercynite lamellae within magnetite. Open circles toward the Fe_3O_4 vertex are averaged analyses (broadened microprobe beam) of host magnetite plus lamellae. Triangles near the Fe_3O_4 vertex (host) are homogeneous magnetite and host magnetite between exsolution lamellae. The single point toward left center of the diagram is one unusually Mg-rich composition of host magnetite plus spinel lamellae (analysis MtH1).

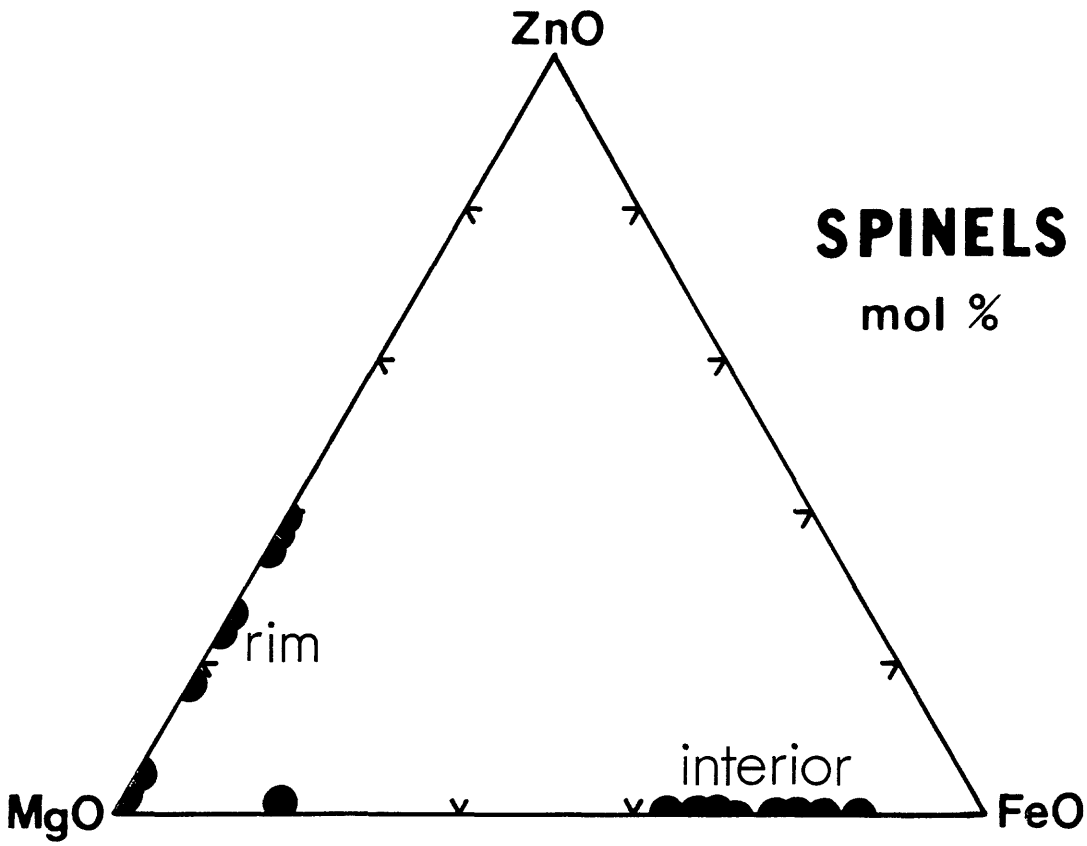

Figure 6. Triangular MgO-ZnO-FeO plot, in mole fractions, of divalent cation compositions of spinels, from structural formulae computed from microprobe analyses. Solid circles represent compositions of analyzed spinels, including homogeneous single-phase spinels, and averaged host plus lamellae compositions. Points along FeO-MgO join near FeO vertex (interior) are compositions of magnetite within teardrop interior, including both homogeneous magnetite and averaged host plus lamellae compositions. Points near MgO vertex and along MgO-ZnO join (rim) are compositions of magnesioferrite near teardrop rim. Single point along MgO-FeO join near MgO vertex is one analysis (MtH1) of host magnetite with spinel lamellae which, because of high MgO content in the lamellae, actually plots closest to magnesioferrite end-member composition.

search, some or all of these metals also may be discovered to be incorporated into minerals of the slag. None of these volatile elements occurred in apparent excess in the trace element analysis (Table 3) or in energy dispersive X-ray analysis of the teardrop; however, in both of these analytical techniques the zinc-rich minerals also did not stand out because of their localized occurrence in a minor portion of the teardrop.

Table 10 is a summary of selected data on the compositions of intergrown or adjacent oxide mineral pairs: magnesioferrite plus hematite, and magnetite plus hematite. Element distribution between coexisting mineral phases generally showed little systematic variation. Most elements analyzed were either present at only trace levels in both phases (for example, Ca and Si), or were abundant in one phase but present at only minor or trace levels in the other: for example, Mg, Mn, and Zn were concentrated in the spinels, and Ti was concentrated in hematite. The only element aside from Fe that was present in large amounts in both spinel and hematite phases was Al; and as shown in Table 2, the only significant variation observed appears to be an increased Al content in two analyses (Y3 and E1) of hematite associated with Al-enriched magnesioferrite. The relatively constant distribution of Mg, Al, Mn, and Ti between the apparently coexisting oxides is a potential source of information on the average temperature and oxygen fugacity at which the minerals crystallized, and this can be explored in future work.

Table 10. Microprobe analyses of coexisting mineral crystals

[The first tabulation of coexisting mineral pairs is for magnesioferrite and hematite pairs (see Tables 4 and 9) towards the rim of the teardrop. The second set of analyses is for pairs of coexisting magnetite and hematite (see Table 5). The magnetite in analysis X5 was homogeneous and free of hercynite exsolution (see Table 6); all other magnetite analyses listed are of averaged magnetite plus contained hercynite spinel lamellae (see Table 7). Analysis pairs are identified by the analysis labels of spinel followed by hematite; for example, F1,F1 is spinel analysis MfF1 and hematite analysis HmF1]

Analysis Pairs	MgO, wt. %		Al_2O_3, wt. %		TiO_2, wt. %	
	spinel	hematite	spinel	hematite	spinel	hematite
F1,F1	11.94	0.10	2.96	0.81	0.04	0.05
F1,Y1	11.94	0.07	2.96	0.87	0.04	0.28
Y1,Y2	12.52	0.05	2.04	0.68	0.00	0.05
F2,F2	12.62	0.16	2.70	0.42	0.00	0.04
X1,X1	17.75	0.16	2.03	0.49	0.01	0.04
5Y,Y3	19.26	0.11	10.34	2.54	0.00	0.13
E1,E1	21.49	0.02	12.19	2.53	0.01	0.04
C1,C1	21.72	0.16	2.40	0.69	0.00	0.10

Analysis Pairs	MgO, wt. %		Al_2O_3, wt. %		TiO_2, wt. %	
	magnetite	hematite	magnetite	hematite	magnetite	hematite
X5,X5	2.70	0.49	10.77	3.89	0.18	7.56
X4,X4	3.50	0.40	11.67	4.22	0.21	5.56
X3,X3	4.15	0.25	14.73	5.31	0.07	1.62
A1,A1	4.43	0.62	14.78	4.18	0.21	7.47
B1,B2	4.75	0.50	13.92	3.93	0.17	6.44
K1,K1	4.80	0.38	17.29	3.94	0.34	6.06
D2,D2	4.92	0.28	12.41	5.06	0.00	2.82
D1,D1	5.72	0.48	15.03	5.04	0.01	4.62
I1,I1	6.00	0.56	16.72	4.07	0.06	5.50
Y4,Y4	6.15	0.29	20.71	4.54	0.08	3.08
J1,J1	6.23	0.58	17.65	4.22	0.12	4.51
G1,G1	6.48	0.54	16.97	4.53	0.05	3.70
G1,G2	6.48	0.60	16.97	6.59	0.05	4.83
D3,D3	7.36	0.53	16.90	5.20	0.04	4.17
H1,H1	16.73	0.23	21.72	3.88	0.02	0.55

PARAGENESIS OF MINERALS IN THE SLAG

Iron-rich minerals in the slag are variable and complex. In part, this may reflect changing conditions of combustion, particularly in changing temperature and partial pressure of carbon monoxide and its substantial effect on the oxidation state of iron in the various minerals. An example of this occurs towards the outer rim of the teardrop where magnetite is less abundant and hematite is predominant, suggesting a slight increase in oxidation during initial cooling of the droplets. In the interior of the teardrops, hematite and magnetite crystallized simultaneously, as indicated by the common intergrowth structures (Figure 7). With subsequent cooling, the hercynite phase exsolved from the magnetite. The original composition of the magnetite thus is represented by those analyses in Table 7, where the microprobe beam was broadened to include both the magnetite and the spinel exsolution lamellae.

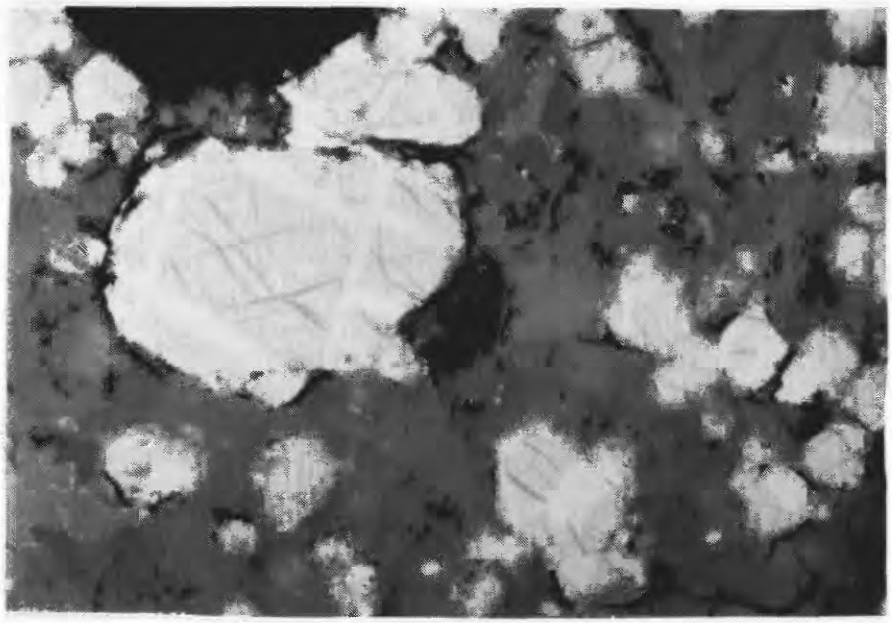

Figure 7. Reflected light photomicrograph of phases of iron oxides. Dimensions of the largest grain are 120 by 65 μm. Grain is predominantly magnetite (gray phase) with intergrown hematite plates (lightest phase), which are 3 to 7 μm in width. Magnetite contains crystallographically oriented exsolution lamellae of hercynite spinel (dark gray phase), 1 μm or less in width.

Iron-rich minerals and anorthite are larger in their grain size than minerals that constitute the groundmass of the slag, a minor portion of which is still glassy. This grain size difference indicates that the former phases crystallized first from the melt, followed by phases of silica and probably minor amounts of potassium feldspar. As this occurred, the composition of the melt changed from an initially mafic basalt to a silica-rich, probably rhyolitic-like melt, with an accompanying increase in viscosity.

The silicate constituents in the slag comprise the silica polymorph minerals, feldspar, and clinopyroxene. Co-occurrence of the three silica polymorphs, tridymite, alpha quartz, and cristobalite, results from the high viscosity of the residual melt that, upon cooling, allowed the crystallization of high entropy forms, cristobalite and tridymite, within the stability range of quartz, $<870^{o}C$ (Carmichael and others, 1974). Alkali feldspars occur in the unheated precursor shale and siltstone, but are not abundant in the slag because of the loss of Na and K during the intense heating of the originally K-rich siltstone and shale, containing respectively, 2.8 and 2.1 weight percent K and 0.6 and 0.5 weight percent Na geometric means (Hinkley and others, 1978).

Phosphorus occurs in the slag teardrops principally as calcium phosphate (apatite?) located in vugs in the teardrop. It, thus, is one of the last phases to crystallize. These crystals may have formed from an immiscible phosphate phase of the melt in a situation similar to that described by Bentor and others (1981), for naturally combusted oil shale. However, it is also possible that the phosphate mineral and clinopyroxene, along with other vug minerals, formed as condensates from hot gas in the vugs.

ORIGIN OF THE SLAG

The origin of the iron-rich slag is puzzling. The simple source of iron would seem to be the bulk iron in the sedimentary rocks immediately overlying the coal; however, these rocks are low in iron, seldom more than about 4 percent Fe_2O_3 by weight (Hobbs, 1980) and averaging considerably less than this amount. Furthermore, iron-containing minerals in the overlying rocks occur as small and well-disseminated grains. It is unlikely that large amounts of iron could be released from this source to run together in a mass sufficient to permit flow of the slag. Note that with this low bulk-iron content, a volume of source rock 10 to 20 times that of the slag, which averages 40 percent iron oxide in composition, would have to lose its entire iron content to furnish iron for the slag.

An alternative source of iron is local pyrite-rich zones in the rocks that overlie the coal seams (B. Kent, oral commun., 1984) or local, iron-rich, usually sideritic, concretions that also have been noted in these rocks (J. McNeal, oral commun., 1985). Siderite occurs in rocks that are overburden to the coal seam in 0.45 and 0.12 percent of the composition of the siltstones plus shales and in dark shale samples, respectively, whereas pyrite constitutes 0.88 and 2.6 percent, respectively, of the arithmetic mean concentration of the same rocks (Hinkley and others, 1978). In the case of organic-rich dark shale, the observed range in pyrite concentration reported by these workers was 0 to 6.8 percent, indicating that substantial amounts of pyrite occur in the shale overlying the coal seams. In the baked, sintered shale (Figure 1), nodules of hematite are visible. Presumably, prior to heating, this volume was filled with a framboidal pyrite nodule that subsequently was converted to hematite during the oxidative heating. Note the hollow centers of the nodules of hematite crystals, which results because the iron as Fe_2O_3 occupies only 63 percent of the volume of the iron as pyrite. However, even with this potential source of iron, the actual mechanism for incorporation of iron into the slag is unclear, because the oxidation of pyrite to hematite, with subsequent loss of sulfur as SO_2, occurs in place and requires no subsequent movement of iron.

Not all of the rock melts. At these temperatures of at least 1250°C apparently it is the iron-rich portion of the rock that has a lower melting point than the remainder of the shale, which sinters. In one of the rock samples, incipient mobilization of the iron is evident (Figure 8). This structure suggests that iron enrichments occur in local concentrations of several millimeters to centimeters in size and that the iron-rich slag seeps out along bedding planes of blocks of rock that have fallen into the combustion cavities or chimneys. The molten material drips into low parts of the cavities where it accumulates in puddles. When the cavity bottom is disturbed through further subsidence, the puddle of still molten slag flows into a lower location where, presumably, it is cooler and the slag congeals. The presence of other elements, particularly P, Ca, and Mg, probably helps the formation of the liquid by lowering the melting point and the viscosity of the melted material. Alkali elements would also aid fluxing, but most of these elements, if present, would have been lost through volatilization in the hottest zones. The low silica content and high iron content are the dominant effects keeping the viscosity low, aiding flow, and facilitating the segregation of the melt from the parent rock.

It is not surprising that an iron-rich melt forms during the heating of the rock, at least where iron-rich zones are present in the parent rock.

Alumina-rich shale is a refractory composition; for example, the equilibrium solidus temperature in the system Al_2O_3-SiO_2 (mullite-cristobalite-liquid) is 1595°C, whereas the solidus temperatures in the systems FeO-SiO_2 and FeO-Fe_2O_3-SiO_2 are 1175 and 1140°C, respectively (Levin and others, 1974).

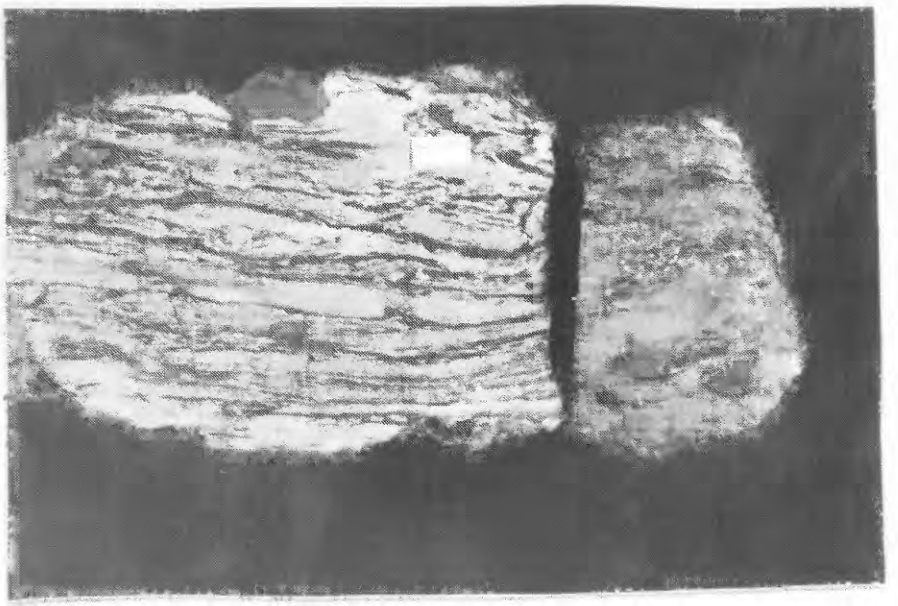

Figure 8. Rock sample showing incipient flow after initial melting of iron-rich slag. Host rock is a carbonaceous shale, with fossil leaf prints still evident. Note that the slag has oozed out at locations where bedding is apparent in shale. Bedding is well developed in unbaked, fissile shale; separated bedding planes presumably serve as zones along which molten slag can migrate, rather than crossing bedding in the shale.

DISCUSSION

Clearly, the slag system was heated intensely and cooled somewhat slowly. The phase relations of the observed mineral assemblages in the slag and in the baked shale potentially provide evidence of the maximum temperature attained, but precise estimates of temperature are subject to many uncertainties. The existence of cordierite, mullite, and cristobalite, based on the respective equilibrium stabilities of these minerals in simple chemical systems, have been used to infer temperatures in coal burns exceeding 1345°C, 1425°C, and 1470°C, respectively (Chatterjee and Ray, 1946; and Reverdatto, 1973). However, as Hooper (1982) has pointed out, all of these minerals may form metastably at considerably lower temperature during the heating and dehydration of clay minerals in the shales. Several temperature constraints can be inferred from the observed extent of solid solution between the iron oxide minerals. The observed maximum content of Al_2O_3 in hematite (8.2 mole percent, analysis HmX3) requires temperatures in the range 800°C to 1100°C, based on phase equilibria in the systems $FeO-Fe_2O_3-Al_2O_3$ (Turnock and Lindsley, 1961) and $Fe_2O_3-Al_2O_3$ (Muan, 1958). The high content of the $MgAl_2O_4$ component observed in magnetite (47 mole percent $MgAl_2O_4$ in analysis HcX1 of averaged host magnetite plus exsolution lamellae) requires a temperature of not more than 950°C, which is the temperature of the crest of the solvus curve in the $Fe_3O_4-MgAl_2O_4$ system for coexisting magnetite plus spinel in equilibrium with hematite (G. S. Mattioli and B. J. Wood, personal communication, 1985; see also Mattioli and Wood, 1985). The observed maximum TiO_2 content in hematite (7.4 atomic percent Ti in hematite intergrown with magnetite, analysis HmX5) may also permit estimation of temperature from equilibria in the $FeO-Fe_2O_3-TiO_2$ system, though significant Mg and Al are also present. We have no unambiguous evidence from the mineral compositions or phase relations for temperatures exceeding 900 to 1000°C, but the observable minerals may only record subsolidus temperatures obtained during the cooling of the slag droplets.

The formation of the iron-rich silicate melt itself must have required temperatures at least exceeding 1100°C; the equilibrium solidus temperature in the system $FeO-SiO_2$ (coexisting fayalite + tridymite + liquid) is about 1175°C (Bowen and Schairer, 1932), and the $FeO-Fe_2O_3-SiO_2$ minimum melting temperature (coexisting fayalite-magnetite-tridymite-liquid) is 1140°C (Osborn and Muan, 1960). The absence of Na_2O in the cooled slag, presumably due to loss by volatilization, is also evidence for the extremely high temperatures attained, but does not permit determination of these temperatures. Further evidence of high temperatures is provided by experimental heating of some of the droplets in a furnace in air. The droplets required a temperature of 1267°C before they deformed plastically when squeezed. Actual flow in the environment where the droplets were created must require a higher temperature. We note also that the natural slag droplets, when removed from the furnace at this high temperature and allowed to cool quickly at room temperature, congealed into a glass-like substance. Glass is notably absent in the droplets as obtained in the field, therefore natural cooling occurred much slower than in our experimental furnace studies.

The obviously very fluid nature of the slag, manifested by flow and dripping as centimeter-size droplets, is indicative of a low viscosity compared to most natural lavas. The low viscosity results from either the iron-rich bulk composition or unusually high temperatures. Natural basaltic

lavas typically have a Newtonian viscosity of approximately 1000 poises (g s^{-1} cm^{-1}) at a typical maximum eruption temperature of about 1200°C (Carmichael and others, 1974, p. 145; Macdonald, 1972, p. 64). The apparent fluidity of the slag droplets suggests a viscosity lower than that of the typical basaltic lava flow, perhaps more comparable to that of remelted lava that drips and forms stalactites in the roof of an active lava tube, where it has been superheated by exposure to burning gases above the lava. Viscosity of a silicate melt composition as a function of temperature can be estimated from the empirical mathematical model of Bottinga and Weill (1972). This has been computed for the bulk composition of the slag as given in Table 1 and is listed in Appendix 2. The results, however, are greatly dependent on the partial molar parameters assumed for the effect of Fe_2O_3 on the viscosity of this iron-rich melt. Bottinga and Weill found little or no reliable data on which to compute the effect of ferric iron on silicate melt viscosity; they provisionally suggested that Fe_2O_3 be assumed to behave identically to FeO. Recent data, however (for example Mysen and others, 1985), suggest that Fe^{+3} in silicate melts behaves dominantly as a network-forming cation, like Al^{+3}, rather than as a network-disrupting cation like Fe^{+2}, and that its effect is to increase the viscosity of a melt rather than to decrease it. The viscosities shown in Appendix 2 have been computed for both assumptions; the range of variation is considerable, more than an order of magnitude. Computed viscosities of the slag are between approximately 140 and 9000 poises at 1200°C, 30 to 1200 poises at 1300°C, 10 to 400 poises at 1400°C, and 4 to 200 poises at 1500°C. The same computation on the Talasea, New Britain, basalt used as a reference in Table 1 gives viscosities in the range 800 to 1100 poises at 1200°C, 190 to 260 poises at 1300°C, 60 to 90 poises at 1400°C, and 40 to 50 poises at 1500°C. Also, undegassed lava prior to or during eruption has its viscosity additionally decreased due to the presence of dissolved H_2O, which is very effective in depolymerizing the network of silicate tetrahedra in the melt. Assumptions about the effect of ferric iron on viscosity are of relatively little importance in most natural igneous rock compositions because the Fe_2O_3 content does not normally exceed a few weight percent; but they are very significant for the extremely ferric iron-rich slag. Another factor to be considered is that the slag likely had a higher Fe^{+2}/Fe^{+3} ratio when it was completely molten at its highest temperature before it began to crystallize, due to the natural trend of reaction between Fe^{+2}, Fe^{+3}, and oxygen on cooling as is discussed below. Assuming that the actual viscosity of the molten slag was somewhere between the two extremes computed in Appendix 2, but probably closer to the higher values, the observed morphology of the slag droplets seems most consistent with a temperature of perhaps 1300-1400°C, several hundred degrees higher than that of typical basaltic lava.

Near surface cooling keeps the partial pressure of volatile elements or compounds relatively low, compared to magmatic systems; hence, the effect of volatiles in lowering crystallization temperatures is minimal. Also, the low confining pressure would keep the volatiles from combining with the melt. This is especially true for the large amount of water vapor and for the still larger amount of carbon dioxide that accompany the natural combustion of the coal.

The iron oxide minerals in the slag are indicative of relatively oxidizing conditions, at least at this particular location within this coal burn. The magnetite-plus-hematite assemblage, if the two phases were of ideal composition, would exactly constrain the oxygen fugacity to the equilibrium values as determined in the pure $FeO-Fe_2O_3$ system. This requires a fairly high fugacity of oxygen, especially at high temperatures (see, for example,

Muan and Osborn, 1962, figure 1). The actual phases, containing Mg, Al, and Ti, are not of ideal composition, so the actual oxygen fugacities would have differed somewhat (but probably not greatly) from that predicted from the pure system. The experimental phase equilibrium data (Muan and Osborn, 1962) show that higher temperatures require increasingly higher oxygen fugacities to stabilize the magnetite-hematite assemblage; thus, at 950°C, magnetite-hematite will coexist at $fO_2 = 10^{-6}$ atm, whereas at 1250°C it requires $fO_2 = 10^{-2}$ atm, and above 1390°C this assemblage would require an oxygen fugacity exceeding that of the Earth's atmosphere. This means that, although magnetite plus hematite is the assemblage now observed in the crystallized slag droplets, it is likely that the completely molten slag originally contained a higher proportion of ferrous iron. For example, using the pure $FeO-Fe_2O_3$ system as a model, a pure iron oxide melt at an oxygen fugacity of 10^{-22} atm (that is, in equilibrium with gas having an oxygen content of about 1/20 that of the atmosphere) would be completely molten above about 1590°C; on cooling below that temperature it would completely crystallize to solid magnetite, and would remain as magnetite until it had cooled to about 1250°C, at which temperature the crystalline magnetite would be converted to hematite. Our observation of magnetite plus hematite, both of which appear to have crystallized from the molten slag and remained stable as the droplets cooled, indicates an oxygen fugacity within a range significantly below that of air, but also considerably above the much more reducing environment of a crystallizing basaltic lava.

Some of the iron oxides within the teardrops occur as globule-like (about 200 μm in diameter) intergrowths of magnetite and hematite, suggesting that these may have originally formed as immiscible droplets of FeO-rich melt within the completely molten teardrop. These oxides also line the vesicles in the teardrop, and the hematite, which is more abundant towards the rim of the teardrop, appears to be replacing magnetite in the vesicle lining, suggesting that the conditions upon cooling became more oxidizing.

The environment of natural coal burns is both varied and capricious. Two common industrial processes, brick and steel fabrication, are similar to natural coal burns. In the case of bricks, clay is fired to a point of slaking and induration. As in clinker, there is a color change in firing bricks as the iron is oxidized to the ferric state. In the case of steel production, ferric iron is reduced in an atmosphere of carbon monoxide, the same gas that reduces ferric iron in clinker and produces mixtures of ferric and ferrous valences. A difference is that in steel production the iron is reduced even further to elemental iron. It is possible that this state of iron does exist in some clinker, especially if the partial pressure of carbon monoxide in the combustion gas was particularly high, and elemental iron may be discovered with diligent search.

CONCLUSION

Thermally altered rocks produced from natural coal burns provide a unique opportunity to examine mineral phase relations at extremely high temperatures, but at unusually low pressure for those temperatures. This study has focused on iron-rich phases in a few teardrops taken from but one slag; examination of similar slags may reveal many other phases of interest as well. A unique substitution of Zn in one of the iron oxide phases has been described and substitution of other volatile metals may well have occurred. In the iron-rich phases, at least four different iron oxide phases are present in the slag teardrops: hematite, magnetite, zinc-bearing magnesioferrite, and hercynite, as lamellae within magnetite.

The four observed iron oxide phases, which formed in the slag teardrops as they crystallized and cooled, record their history of falling temperature and increasingly oxidizing conditions in contact with the gas on the exterior of the slag droplets. Magnetite, $(Fe^{+2}, Mg)(Fe^{+3}, Al)_2O_4$, and hematite, $(Fe, Al, Ti)_2O_3$, crystallized first, either from the bulk slag or from immiscible droplets of iron oxide melt. The large extent of solid solution of Mg, Al, and Ti in the magnetite and hematite is indicative of the high temperature of their formation. As the solidified droplets cooled, the high initial Mg and Al content of the magnetite resulted in the exsolution of hercynite spinel, $(Fe^{+2}, Mg)(Al, Fe^{+3})_2O_4$, within the magnetite, a feature not normally seen in the magnetite of basaltic lavas. The formation of the assemblage magnesioferrite spinel, apparently $(Mg, Zn)(Fe^{+3}, Zn, Al, Mn^{+3})_2O_4$, plus hematite that is nearly pure, except for minor Al, with all the iron in the ferric state in both phases, apparently occurred at the surface of the droplets due to equilibrium with very oxidized gas as the droplets were cooling.

ACKNOWLEDGMENTS

Ray Wilcox performed the optical analysis of the clinopyroxene; Don Williamson provided the Mossbauer analysis of the teardrops; and Larry Jackson provided a definitive analysis of the FeO content of the droplets. Faith Rogers assisted in collection of the specimens in the field, and the Kerr-McGee Coal Company allowed access to their Jacobs Ranch Mine. Jim McNeal provided helpful discussion of pyrite nodules. R. Grauch, R. Wilcox, and L. Carter provided helpful reviews.

REFERENCES

Bentor, Y.K., Kastner, M., Perlman, I., and Yellin, Y., 1981, Combustion metamorphism of bituminous sediments and the formation of melts of granitic and sedimentary composition: Geochim. et Cosmochim Acta, v. 45, p. 2229-2255.

Bottinga, Yan, and Weill, Daniel F., 1972, The viscosity of magmatic silicate liquids: a model for calculation: American Journal of Science, v. 272, p. 438-475.

Bowen, N.L. and Schairer, J.F., 1932, The system, Feo-SiO_2: American Journal of Science, v. 24, p. 405-455.

Carmichael, I.S.E., Turner, F.J., and Verhoogen, J., 1974, Igneous petrology: New York, McGraw-Hill, 739 p.

Ceely, F.J. and Daman, Ernest L., 1981, Combustion process technology, in Chemistry of coal utilization, Second Supplementary Volume, M.A. Elliot, ed., New York, Wiley Interscience, p. 1313-1387.

Chaterjee, N.N., and Ray, S., 1946, On the burnt coal outcrop from the Central Kujama Colliery, Jharia, Quarterly Journal Geological, Mineralogical, and Metallurgical Society of India, v. 18, p. 133-135.

Craig, Jerald N. II., Burns, L.K., Ethridge, F.G., Laughter, T.F., and Youngberg, A.D., 1982, Overburden characteristics and post-burn studies at the Hanna underground gassification site: stratigraphy, depositional environment, and mineralogy of the Hanna Formation: U.S. Dept. of Energy, DOE/LC/10496-T1.

Coates, D.A. and Naeser, C.W., 1984, Map showing fission-track ages of clinker in the Rochelle Hills, southern Campbell and Weston Counties, Wyoming: U.S. Geological Survey, Misc. Investigation Map I-1462.

Cosca, Michael A., Peacor, Donald R., and Essene, Eric J., 1985, The chemistry and structure of a natural ferrialuminum tschermakitic pyroxene produced by pyrometamorphism: Geological Society of America, Abstracts with Programs, v. 17, p. 553.

Herring, J.R., 1986, Emissions from natural coal fires: manuscript.

Herring, J.R. and Rich, F.J., 1983, Spontaneous coal combustion; mechanisms and prediction: Proceedings of 1983 International Conf. on Coal Science, Pittsburgh, Pa., Int'l. Energy Agency, p. 753-756.

Hinkley, T.K., Ebens, R.J., and Boerngen, J.G., 1978, Overburden chemistry and mineralogy at Hanging Woman Creek, Big Horn County, Montana, and recommendations for sampling at similar sites in Geochemical Survey of the Western Energy Regions: U.S. Geological Survey Open-File Report 78-1105, p 150-168.

Hobbs, Robert G., 1980, Analyses of coal and selected rock samples from the U.S. Geological Survey 1975 drilling, Recluse geologic analysis area, northern Campbell County, Wyoming: U.S. Geological Survey Open-File Report 80-1161, 78 p.

Hooper, Robert L., 1982, Mineralogy of a coal burn near Kemmerer, Wyoming: Washington State Univ., Pullman, M.S. Thesis, 79 p.

Lapham, Davis, Barnes, John, Downey, Jr., Wayne, and Finkelman, Robert, 1980, Mineralogy associated with burning anthracite deposits of eastern Pennsylvania: Pennsylvania Geological Survey, Mineral Resource Report 78, 82 p.

Levin, E.M., Robbins, C.R., and McMurdie, H.F., 1974, Phase diagrams for ceramists, 3rd ed., American Chemical Society, 601 p.

Lowder, G.G. and Carmichael, I.S.E., 1970, The volcanoes and caldera of

Talasea, New Britain: geology and petrology: Geological Society of America, Bulletin, v. 81, p. 17-38.
Macdonald, G.A., 1972, Volcanoes: Englewood Cliffs, N.J., Prentice-Hall, 510 p.
Mattioli, G.S., and Wood, B.J., 1985, Activities and volumes in $MgAl_2O_4$-Fe_3O_4-$\gamma Fe_{8/3}O_4$ spinels: implications for mantle oxygen fugacity: Geological Society of America, 98 Ann. Mtg., Abstracts, v. 17, p. 655.
Muan, Arnulf, 1958, On the stability of the phase $Fe_2O_3.Al_2O_3$: American Journal of Science, v. 256, p. 413-422.
Muan, Arnulf, and Osborn, E.F., 1962, Phase equilibria as a guide in refractory technology: American Ceramic Society, Bulletin, v. 41, p. 450-455.
Mysen B.O., Virgo, D., Scarfe, C.M., and Cronin, D.J., 1985, Viscosity and structure of iron- and aluminum-bearing calcium silicate melts at 1 atm: American Mineralogist, v. 70, p. 487-498.
Osborn, E.F., and Muan, Arnulf, 1960, Phase equilibrium diagrams of oxide systems, Plate 6: American Ceramic Society and the Edward Orton, Jr., Ceramic Foundation.
Powers, D.A. and Frazier, A.W., 1976, VISRHO: a computer subroutine for estimating the viscosity and density of complex silicate melts: Sandia National Laboratory, Rept. SAND76-0649.
Reser, M.K., ed., 1974, Phase diagrams for ceramists, 3rd ed.: American Chemical Society, 601 p.
Reverdatto, V.V., 1970, The facies of contact metamorphism: Australian National University, Canberra, Geological Publication No. 233, p. 87-89.
Rogers, G. Sherburne, 1917, Baked shale and slag formed by the burning of coal beds: U.S. Geological Survey Professional Paper 108, 10 p.
Turnock, A.C., and Lindsley, D.H., 1961, Fe-Al and Fe-Ti spinels and related oxides, Ann. Rept. Director Geophys. Lab., in Carnegie Inst. Washington Year Book, v. 60, p. 152-157.

APPENDIX 1.

Electron microprobe analyses were performed on an ARL-SEMQ (any use of trade names is for descriptive purposes only and does not imply endorsement by the U.S. Geological Survey) automated microprobe using 15 KV accelerating voltage, 100 μA emission current, 64 nA beam current, and 10 nA sample current. Beam diameter, when sharply focused was about 1 μm, however to obtain averaged compositions of magnetite containing hercynite exsolution lamellae, some analyses were made with the beam diameter broadened to between 20 and 30 μm. The probe data were reduced using the MAGIC-IV correction program. Standards used for the analysis were spinel for Mg and Al; titanomagnetite for Ti and Fe; manganese-bearing fayalite for Si and Mn; gahnite for Zn; and multicomponent silicate glass for Ca. Counting times were 20 to 80 seconds on element peaks and 20 to 40 seconds on backgrounds. Minimum detection limits and 3σ estimates of analytical accuracy, computed from counting statistics, varied within the following ranges in weight percent:

Oxide	Minimum Detection Limit	Analytical Error (3σ) for analyses with low element concentration	Analytical Error (3σ) for analyses with high element concentration
MgO	0.04-0.07	0.08-0.11	0.25-0.60
Al_2O_3	0.10-0.12	0.12-0.18	0.30-1.00
SiO_2	0.05-0.09	0.08-0.14	---
CaO	0.02-0.05	0.04-0.08	---
TiO_2	0.02-0.06	0.02-0.09	0.19-0.26
MnO	0.03-0.04	0.04-0.06	0.16-0.20
FeO	0.04-0.05	---	0.40-1.00
ZnO	0.09-0.24	0.13-0.36	0.60-0.90

Ranges are given because the detection limits and analytical precision vary with counting time, concentration of the element being analyzed, and matrix composition of the mineral grain. In the analyses of iron oxide phases, Tables 4-9, measured values that did not exceed the appropriate minimum detection limit are reported as [0]. All the analyses given in Tables 4-10 are for iron oxide phases from a single polished sample (teardrop mount #2).

A limited number of partial microprobe analyses on a second polished sample gave a similar range of compositions, in weight percent: hematite-- 0.1 to 0.4 MgO, 0.3 to 3.0 Al_2O_3, 0.0 to 5.6 TiO_2; magnetite-- 2 to 4 MgO, 4-11 Al_2O_3; magnesioferrite-- about 20 MgO, 1 to 2 Al_2O_3, and 0.5 Zn. No high-Zn magnesioferrite was observed in this sample.

Appendix 2.--Viscosity Calculation

Estimated viscosity of molten slag and basalt computed using the model of Bottinga and Weill (1972). Newtonian viscosity is given in poises.

Method	$XSiO_2$	1200°C	1300°C	1400°C	1500°C
Slag					
A-50	0.53	140	30	10	4
A-60	0.53	260	40	10	10
B-50	0.64	5400	700	300	90
B-60	0.64	9200	1200	400	200
Talasea Basalt:					
A-60	0.59	800	200	70	40
B-60	0.60	1100	300	90	50

Slag and basalt compositions are given in Table 1. The coefficients of Bottinga and Weill (1972) are used when available; the coefficients for the components $KAlO_2$ and 1/2 P_2O_5 are assumed to be equal to those of $NaAlO_2$ and SiO_2 as suggested by Bottinga and Weill; the coefficients for $MnAl_2O_4$ is assumed to be equal to that of $CaAl_2O_4$, and other coefficients not given by Bottinga and Weill at certain temperatures are taken from those assumed by Powers and Frazier (1976); the coefficient for Al_2O_3 not associated as $MAlO_2$ or MAl_2O_4 species is assumed to take the value $-5.17 + 9479/T$ (°C) suggested by Powers and Frazier, though this expression was only derived from melts with $0.35 \geq XSiO_2 \leq 0.45$, and the coefficient for Fe_2O_3 is assumed to have the same value as Al_2O_3. Other assumptions made: method A-50, all Fe_2O_3 is assumed to behave as 2FeO, and coefficients derived for the range of SiO_2 mole fraction $0.45 \geq XSiO_2 \leq 0.55$ are used; method A-60, Fe_2O_3 is treated the same as 2FeO and coefficients derived for $0.55 \geq XSiO_2 \leq 0.65$ are used; method B-50, all Fe_2O_3 is assumed to behave as Al_2O_3, and coefficents for $0.45 \geq XSiO_2 \leq 0.55$ are used; and method B-60, Fe_2O_3 is treated as Al_2O_3 and coefficients for $0.55 \geq XSiO_2 \leq 0.65$ are used. As shown in the $XSiO_2$ column of the table above, the calculated mole fraction of SiO_2 in the melt changes when assumption (A) or (B) is made, because the number of other hypothetical species in the melt changes, so that for assumption (A), the slag melt falls into the $0.45 \geq XSiO_2 \leq 0.55$ category of Bottinga and Weill, whereas for assumption (B) it falls into the $0.55 \geq XSiO_2 \leq 0.65$ category. For this reason, computations using the viscosity coefficients for both ranges of silica content are shown.